# Nanoscopic characterization of individual endogenous protein aggregates in human neuronal cells

COMMUNICATION

# Nanoscopic characterization of individual endogenous protein aggregates in human neuronal cells

Daniel R. Whiten[†], Yukun Zuo[†], Laura Calo, Minee-Liane Choi, Suman De, Patrick Flagmeier, David C. Wirthensohn, Franziska Kundel, Rohan T. Ranasinghe, Santiago E. Sanchez, Dilan Athauda, Steven F. Lee, Christopher M. Dobson, Sonia Gandhi, Maria-Grazia Spillantini, David Klenerman*, Mathew H. Horrocks[†]*

***Abstract:*** *The aberrant misfolding and subsequent conversion of monomeric protein into amyloid aggregates characterizes many neurodegenerative disorders, including Parkinson's and Alzheimer's diseases. These aggregates are highly heterogeneous in structure, generally of low abundance, and typically smaller than the diffraction limit of light (~250 nm). To overcome these challenges, we have developed a method to characterize protein aggregates at the nanometer scale without the need for a conjugated fluorophore. Using a combination of DNA PAINT and an amyloid specific aptamer, we demonstrate that this technique is able to detect and super-resolve a range of aggregated species, including those formed by α-synuclein and amyloid-β. Additionally, this method enables endogenous protein aggregates within cells to be characterized. We found that neuronal cells derived from patients with Parkinson's disease contain a larger number of protein aggregates than those from healthy controls.*

Protein misfolding and aggregation is closely associated with the development of many neurodegenerative disorders, such as Alzheimer's disease (AD) and Parkinson's disease (PD)[1]. In AD, the protein tau is deposited in intracellular inclusions[2], while the amyloid beta (Aβ) peptide is in extracellular plaques. Similarly, in PD, aggregates of the protein α-synuclein (αS) are found in Lewy bodies[3] within neuronal cells. There proteins are often heavily

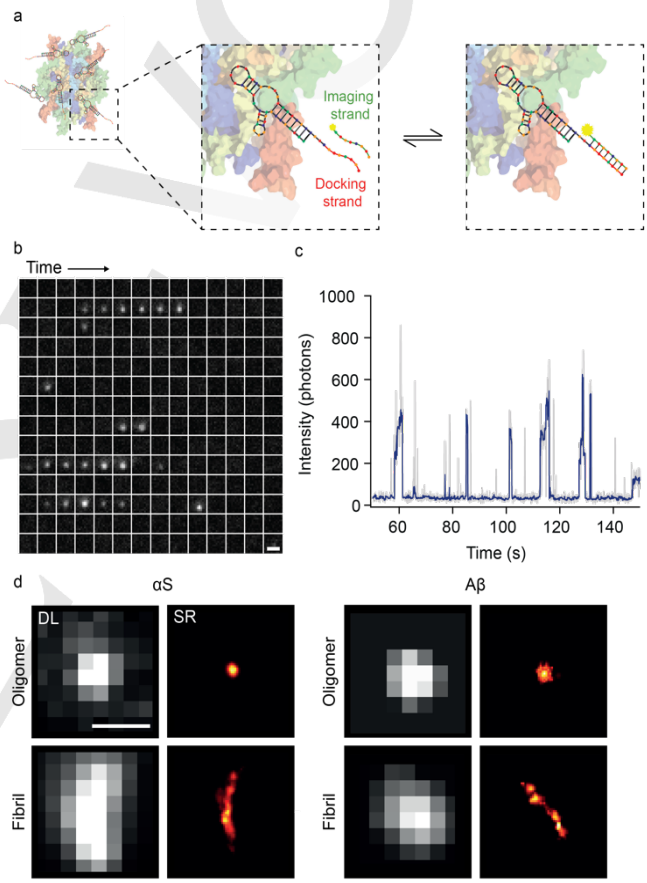


Figure 1. The concept of ADPAINT. (a) Schematic representation of ADPAINT shows an aggregate bound by multiple aptamers. The DNA docking strand (red) on the aptamer is transiently bound by the complementary imaging strand (green) to generate a SR image. (b) Example time montage of an oligomer undergoing ADPAINT. Each sub-image is separated by 0.5 s, moving through time from left to right then top to bottom, and the scale bar is 1 μm. (c) Intensity profile of the oligomer in (b). Each intensity burst represents the binding of the imaging strand to the aptamer. Gray- raw intensity profile, Blue- using a Chung-Kennedy filter[31] with a window of 5 frames applied. (d) Examples of diffraction limited (DL, using Thioflavin-T) and super-resolved (SR, using ADPAINT) images of an αS and Aβ oligomer and fibril. The scale bar is 500 nm.

[*] Daniel R. Whiten, Yukun Zuo, Suman De, Patrick Flagmeier, David C. Wirthensohn, Franziska Kundel, Rohan T. Ranasinghe, Santiago E. Sanchez, Steven F. Lee, Christopher M. Dobson, David Klenerman, Mathew H. Horrocks.
Department of Chemistry, University of Cambridge, Lensfield Road, Cambridge CB2 1EW, UK
Email: dk10012@cam.ac.uk
mathew.horrocks@ed.ac.uk
David Klenerman
UK Dementia Research Institute, University of Cambridge, Cambridge CB2 0XY, United Kingdom
Laura Calo, Maria-Grazia Spillantini.
Department of Clinical Neurosciences, University of Cambridge, Hills Road, Cambridge CB2 0AH, UK
Minee-Liane Choi, Dilan Athauda, Sonia Gandhi.
UCL Institute of Neurology, Queen Square, London WC1N 3BG, UK.
Minee-Liane Choi, Sonia Gandhi.
The Francis Crick Institute, 1 Midland Road, London.
Mathew Horrocks
Current addresses: EaStCHEM School of Chemistry, University of Edinburgh, David Brewster Road, Edinburgh EH9 3FJ, United Kingdom.
UK Dementia Research Institute, University of Edinburgh, Edinburgh, UK.

[†] authors contributed equally
* authors contributed equally

post-translationally modified, for example αS undergoes phosphorylation, nitration and truncation[4–6], making it important to be able to characterize the real endogenous aggregates formed in cells, since these may differ from those formed by unmodified proteins.

More recently, soluble nanometer-sized protein oligomers have been identified as the major cytotoxic species in AD and PD[7–10], but the study of such species has remained challenging, as they tend to be low in abundance and to adopt a wide range of heterogeneous structures. To overcome this problem we have developed an array of single-molecule techniques[11–14] to observe oligomeric species individually, and have applied them to characterize the aggregation pathway of several disease-related proteins *in vitro*. In many such methodologies, the protein of interest needs to be tagged with either an organic fluorophore or a fluorescent protein. This is very challenging for *in vivo* or in cell imaging, and in some cases the label may have an adverse effect on the behavior of the protein[15]. Alternatively, dyes such as thioflavin-T/S (ThT/S) or the pentameric form of formyl thiophene acetic acid (pFTAA), whose fluorescence in each case is enhanced upon binding to amyloid structures, can be used to detect protein aggregates. We have recently used such dyes in combination with total internal reflection fluorescence microscopy (TIRF) microscopy to image individual aggregates in human cerebrospinal fluid (CSF) in a diffraction-limited manner[16]. Such dyes, however, bind to other cellular components limiting their versatility[17], and may not be sensitive to the smaller oligomers, which in addition to being major therapeutic targets, could also be biomarkers for neurodegeneration[16,18]. Furthermore, conventional far-field microscopy techniques face a limit in their resolving capability imposed by the optical diffraction barrier. As many sub-cellular structures are known to be affected by toxic protein aggregates[19,20], it is important to define the morphology and location of aggregates in the cellular milieu in order to understand the interplay between protein aggregation and the loss of cellular homeostasis.

We have employed the use of an aptamer previously reported to recognize oligomers and fibrils formed from αS and Aβ[21] to enable the sensitive and specific visualization of protein aggregates at the nanoscale. Aptamers are single-stranded oligonucleotides developed to have high affinity and specificity, and can be made for almost any molecule or structure[22,23]. The advent of super-resolution (SR) microscopy methods[24] has improved the resolution of optical methods. Recently, an SR method, referred to as DNA PAINT (point accumulation in nanoscale topography), has been developed[25,26]. The technique utilizes short complementary strands of DNA; a "docking" strand is conjugated to an antibody or protein of interest whilst its complementary "imaging" strand is labelled with an organic fluorophore. We have extended the aptamer sequence with a docking strand sequence (Figure 1a, SI Table 1), to generate SR images of protein aggregates (Figure 1d), and we herein refer to this method as Aptamer DNA PAINT (ADPAINT). The repeated transient binding of the imaging strand to the docking strand (Figure 1a,b,c) allows it to be spatially localized, enabling the reconstruction of a SR image. Additional burst montages are shown in SI Figure 2, providing a more complete view of the variation in fluorescent bursts caused by the stochastic binding of imaging strand to the docking strand. DNA PAINT can be realised

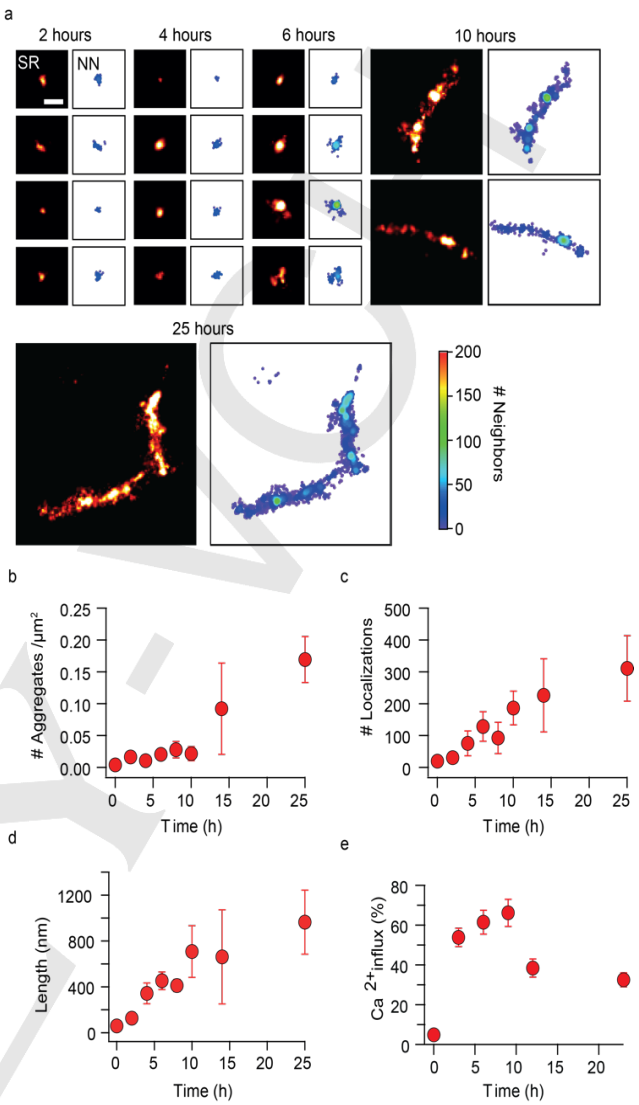


Figure 2. ADPAINT enables the imaging of a range of species formed during the aggregation of αS. (a) Examples aggregates are shown in SR on the left, with their corresponding nearest neighbor plots shown on the right, highlighting hotspots of localization density. The scale bar is 200 nm. (b) The number of aggregates increases over the time-course, and (c) the number of localizations also increases as the species get larger, which is shown by (d) as the mean length increases. Data shown are mean ± SD of three independent aggregation reactions. (e) The percentage of liposomes permeabilized upon addition of aggregates from the different time-points (mean ± SD over 16 FOV (69 x 69 µm)).

using both TIRF microscopy, and more recently, spinning disk confocal microscopy[27]. Examples of oligomers and fibrils of both αS and Aβ imaged using ADPAINT are shown in Figure 1d (full fields of view shown in SI Figures 3 and 4). A control experiment using just the imaging strand (without aptamer) showed little non-specific binding of the imaging strand to the aggregates (SI Figure 5). The aptamer is specific to the conformation of the aggregates, and so these can be detected even amongst an excess of monomer. Furthermore, for primary and secondary antibodies, the size of the probe can add a linkage error of 15 nm[28], whereas the small size of aptamers enables them to bind at a high density,

and at a close proximity to their epitopes, leading to a high imaging resolution, as has also been shown with DNA PAINT and affirmers[29]. Typically, we achieve a localization precision of ~10 nm and a resolution of ~25 nm (SI Table 2), with a limit of detection of ~30 pM of aggregates (Supporting Information). This enables us to quantify the oligomers formed during physiologically relevant aggregation reactions. Each image was acquired over 200 s; however, since PAINT-based techniques are not limited by photobleaching[30], this time can be lengthened to localize a greater number of binding events in order to obtain a higher resolution image of the protein or cellular structure of interest.

To assess the ability of ADPAINT to study the heterogeneity of complex aggregation mixtures, a solution of monomeric αS was incubated under conditions previously described to result in its aggregation[7,11]. At early time-points in the reaction, only a few aggregates were detected, and these were predominantly small (< 400 nm in length for the first 6 h) and rounded, consistent with the expected appearance of oligomers (Figure 2a). After 10 h, fibrils were detected. To visualize the distribution of binding sites within each aggregate, we color-coded the localizations according to their local (typically within 40-50 nm) molecular density. The resulting images show maps of the local molecular density of individual aptamer binding sites, revealing a highly non-uniform distribution, particularly in the later aggregates (right panel in each case). This shows that the aggregate structure is not homogeneous, but instead varies at the nanoscale, a finding that is made possible through this method. Further analysis of the ADPAINT images showed that the number of aggregates increased over time, consistent with the high aggregation propensity of αS (Figure 2b). Unlike with antibodies in which labelling stoichiometrically can be challenging, each aptamer is labelled with a single DNA docking strand allowing for quantitative imaging. We have taken advantage of this by quantifying the number of localizations per aggregate, finding that this increased over time (Figure 2c, SI Figure 6). Additionally, the aggregates also got larger, as indicated by the increase in their mean length (Figure 2d, SI Figure 7).

The permeabilization of membranes has been suggested to be the most ubiquitous toxic mechanism associated with protein aggregates[31–35]. We have recently developed a method to characterize the ability of protein aggregates to permeabilize lipid membranes[8] (details are given in Supporting Information), and have used this within this study, finding that the earlier aggregates caused a higher level of influx compared to those present at later stages of the aggregation process (those around 600 nm in length) (Figure 2e). Additionally, the binding of the aptamer to the aggregates did not inhibit their ability to permeabilize the lipid membranes, and the aptamer itself displayed no propensity to alter these membranes (SI Figure 8). Thus, it appears likely that ADPAINT can be applied to characterize the structures of the pathological aggregates without altering the functional states of the protein or the cell membrane.

We next used ADPAINT to investigate aggregate formation in a cellular model of PD. Missense mutations[13,36–40], and duplications or triplications of the *SNCA* gene, which encodes αS, lead to autosomal dominant early-onset PD[41,42]. It has previously been shown that the formation of αS oligomers *in vitro* is concentration dependent[12], and ADPAINT now enables us to determine whether this dependence is reflected within cellular models that overexpress αS. We made use of induced pluripotent stem cells (iPSCs) from a PD patient with a triplication of the *SNCA* gene, and from a healthy control unaffected by the disease to generate cortical neurons. Although SR methods have been utilized to image fibrils in cells, these are typically exogenously

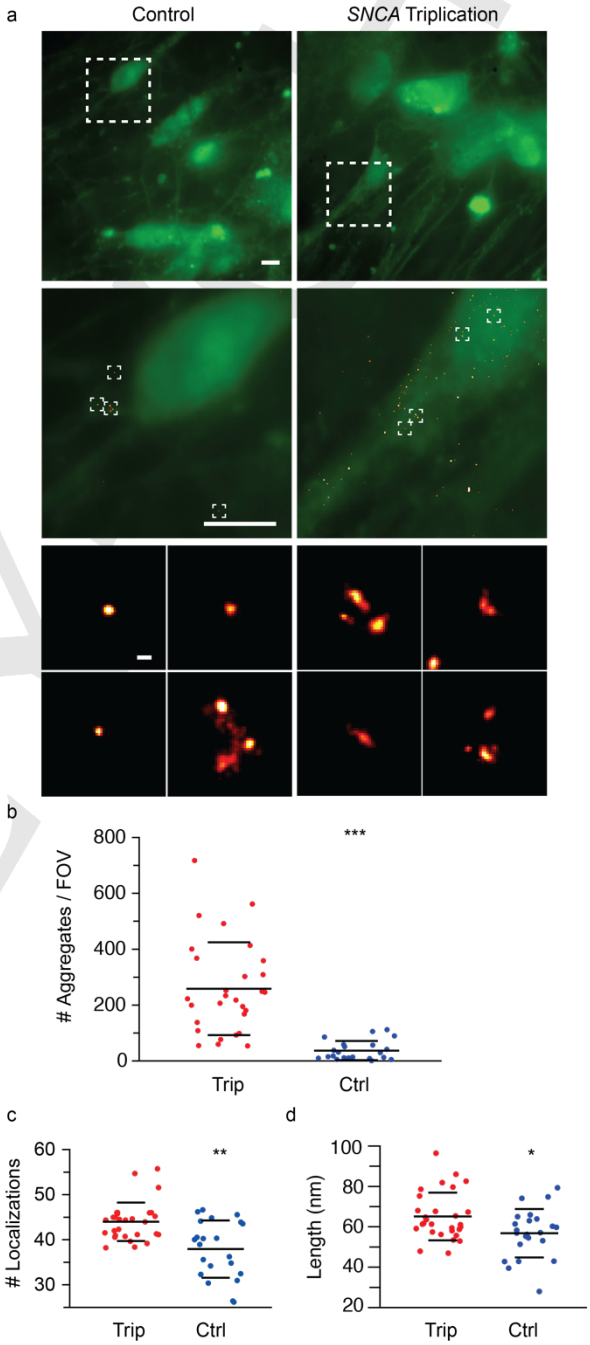


Figure 3. ADPAINT in iPSCs. (a) iPSCs from a PD patient with a triplication of the *SNCA* gene, and a healthy control. Protein aggregates were imaged using pFTAA (green) or ADPAINT (red). The scale bars are 5 μm and 500 nm in the zoom. Compared to control cells, *SNCA* triplication cells show (b) significantly more aggregates and an increase in the (c) number of localizations, and (d) the average length of the aggregates. The data shown are means ± SD of at least 27 fields of view. * $p < 0.05$, ** $p < 0.001$, *** $p < 0.0001$; analyzed by t-test.

added aggregates generated from fluorophore labelled protein[43,44,28,45–47], this is the first case in which a specific probe for aggregates is used, and so enables the SR imaging of unlabeled, endogenous aberrant protein complexes. These were imaged in fixed, permeabilized cells using both ADPAINT at the SR-level, and in a diffraction-limited manner using pFTAA, a dye which recognizes β-sheet structures and becomes fluorescent upon binding to protein aggregates[48,49]. To image at a greater depth into the cells, the illumination was changed to oblique-angle epifluorescence. Figure 3 shows examples of human iPSC-derived neurons with and without the *SNCA* triplication after being plated and stained with pFTAA (green) (further examples are shown in SI Figure 9). PFTAA not only binds to the aggregates, which appear as brighter spots, but also interacts with cellular organelles and membranes, preventing the aggregates from being identified or their precise location within the cell being determined. Unlike pFTAA, the aptamer has a high specificity, and only small clusters of binding events are detected within the cytosol. Due to the background fluorescence being higher in oblique-angle epifluorescence than in TIRF, the resolution we achieved within cells was lower than he resolution achieved for the *in vitro* formed aggregates (SI Table 2). Quantification of these images shows that there are significantly ($p < 0.0001$) more aggregates in the cells derived from the individual carrying a triplication of the *SNCA* locus compared to iPSC-derived neurons from the healthy control. We found that the species detected in these experiments resemble those formed early on in the *in vitro* aggregation pathway (0-2 hours) shown in Figure 2, having ~45 localizations per aggregate (Figure 3c), and being <150 nm in length (Figure 3d). Furthermore, the aggregates detected in the cells having the *SNCA* triplication locus give rise to significantly more localizations (Figure 3c) and are larger (Figure 3d) than those in the healthy control cells. Given the likelihood of toxicity arising directly from these aggregates, this observation could help explain the neuronal cell death associated with PD.

One of the significant advantages of ADPAINT is the ability of the aptamer to selectively bind to protein aggregates and not the excess of monomeric protein which is present in cells. As a comparison, we used the commercially available MJF14-6-4-2 filament antibody, which detects an epitope that is only present in aggregates and not in the monomeric protein[50], and the Alexa Fluor 405 labeled aptamer to detect dual labeled aggregates of αS added to iPSC-derived neurons (SI Figure 10). In the case of the MJF14-6-4-2 antibody, there was non-specific staining of regions of the cell that did not contain aggregated αS, whereas the aptamer only detected dual-labeled aggregates. Furthermore, the larger size of antibodies can add a further 10-15 nm between the target and the labeled probe[28]. When used with DNA PAINT, the same MJF14-6-4-2 antibody (SI Figure 11), was unable to resolve individual aggregates, but instead there was diffuse staining in both the *SNCA* triplication and control cells.

In conclusion, we have developed an SR method to characterize the toxic species formed during neurodegenerative diseases. We have used ADPAINT to characterize both *in vitro* aggregates αS and Aβ, and also endogenous unlabeled oligomers formed in patient-derived neurons. Interestingly, we found that the aggregates formed early in the *in vitro* aggregation closely resemble the morphology of those found within human iPSC-derived cortical neurons, and that these appear to be most responsible for disrupting lipid membranes, Although only imaged at one stage in the lifetime of the iPSC-derived cortical neurons, this method can also be used to determine how such species develop as cells age, potentially yielding further insights into the progression of neurodegenerative diseases.

## Acknowledgements

M.H.H. was supported by a Junior Research Fellowship at Christ's College, University of Cambridge, and the Herchel Smith Foundation. Y.Z. was supported by Cambridge Trust and Chinese Scholarship Council. PF was supported by Boehringer Ingelheim Fonds, and the German National Merit Foundation. S.D. is funded by a Marie-Curie Individual Fellowship. C.M.D. is supported by the UK Biotechnology and Biochemical Sciences Research Council and the Wellcome Trust. This work was also supported by the Cambridge Centre for Misfolding Diseases (P.F., and C.M.D.), the Royal Society (D.K.), the European Research Council with an ERC Advanced Grant (669237) (D.R.W and D.K.), and the Allen Distinguished Investigator Program, through The Paul G. Allen Frontiers Group (M.H.H.). SG is a Wellcome Trust Intermediate Clinical Fellow. M.G.S. and L.C. were supported by the Cambridge Biomedical Research Centre at Addenbrooke's hospital, Cambridge and the Allen Foundation. The authors wish to thank Swapan Preet for purification of protein, and the mechanical workshops within the Department of Chemistry for aiding in the construction of single-molecule instrumentation.

The authors declare no competing financial interest.

**Keywords:** Super-resolution • aptamer • DNA PAINT • neurodegenerative disorders • protein aggregation • α-synuclein • Parkinson's disease • Alzheimer's disease • induced pluripotent stem cells • amyloid formation.

[1] F. Chiti, C. M. Dobson, *Annu. Rev. Biochem.* **2006**, *75*, 333–366.
[2] S. Barghorn, P. Davies, E. Mandelkow, *Biochemistry (Mosc.)* **2004**, *43*, 1694–1703.
[3] M. G. Spillantini, M. L. Schmidt, V. M.-Y. Lee, J. Q. Trojanowski, R. Jakes, M. Goedert, *Nature* **1997**, *388*, 839–840.
[4] P. J. Barrett, J. Timothy Greenamyre, *Brain Res.* **2015**, *1628*, 247–253.
[5] H. Vicente Miranda, É. M. Szego, L. M. A. Oliveira, C. Breda, E. Darendelioglu, R. M. de Oliveira, D. G. Ferreira, M. A. Gomes, R. Rott, M. Oliveira, et al., *Brain J. Neurol.* **2017**, *140*, 1399–1419.
[6] A. Oueslati, M. Fournier, H. A. Lashuel, *Prog. Brain Res.* **2010**, *183*, 115–145.
[7] N. Cremades, S. I. A. Cohen, E. Deas, A. Y. Abramov, A. Y. Chen, A. Orte, M. Sandal, R. W. Clarke, P. Dunne, F. A. Aprile, et al., *Cell* **2012**, *149*, 1048–1059.
[8] P. Flagmeier, S. De, D. C. Wirthensohn, S. F. Lee, C. Vincke, S. Muyldermans, T. P. J. Knowles, S. Gandhi, C. M. Dobson, D. Klenerman, *Angew. Chem. Int. Ed.* **2017**, n/a–n/a.

[9] L. M. Billings, S. Oddo, K. N. Green, J. L. McGaugh, F. M. LaFerla, *Neuron* **2005**, *45*, 675–688.
[10] R. M. Koffie, M. Meyer-Luehmann, T. Hashimoto, K. W. Adams, M. L. Mielke, M. Garcia-Alloza, K. D. Micheva, S. J. Smith, M. L. Kim, V. M. Lee, et al., *Proc. Natl. Acad. Sci. U. S. A.* **2009**, *106*, 4012–4017.
[11] M. H. Horrocks, L. Tosatto, A. J. Dear, G. A. Garcia, M. Iljina, N. Cremades, M. Dalla Serra, T. P. J. Knowles, C. M. Dobson, D. Klenerman, *Anal. Chem.* **2015**, *87*, 8818–8826.
[12] M. Iljina, G. A. Garcia, M. H. Horrocks, L. Tosatto, M. L. Choi, K. A. Ganzinger, A. Y. Abramov, S. Gandhi, N. W. Wood, N. Cremades, et al., *Proc. Natl. Acad. Sci.* **2016**, *113*, E1206–E1215.
[13] L. Tosatto, M. H. Horrocks, A. J. Dear, T. P. J. Knowles, M. Dalla Serra, N. Cremades, C. M. Dobson, D. Klenerman, *Sci. Rep.* **2015**, *5*, DOI 10.1038/srep16696.
[14] S. L. Shammas, G. A. Garcia, S. Kumar, M. Kjaergaard, M. H. Horrocks, N. Shivji, E. Mandelkow, T. P. J. Knowles, E. Mandelkow, D. Klenerman, *Nat. Commun.* **2015**, *6*, 7025.
[15] V. L. Anderson, W. W. Webb, *BMC Biotechnol.* **2011**, *11*, 125.
[16] M. H. Horrocks, S. F. Lee, S. Gandhi, N. K. Magdalinou, S. W. Chen, M. J. Devine, L. Tosatto, M. Kjaergaard, J. S. Beckwith, H. Zetterberg, et al., *ACS Chem. Neurosci.* **2016**, *7*, 399–406.
[17] S. Sugimoto, K. Arita-Morioka, Y. Mizunoe, K. Yamanaka, T. Ogura, *Nucleic Acids Res.* **2015**, *43*, e92–e92.
[18] T. Tokuda, M. M. Qureshi, M. T. Ardah, S. Varghese, S. a. S. Shehab, T. Kasai, N. Ishigami, A. Tamaoka, M. Nakagawa, O. M. A. El-Agnaf, *Neurology* **2010**, *75*, 1766–1772.
[19] D. Snead, D. Eliezer, *Exp. Neurobiol.* **2014**, *23*, 292–313.
[20] L. Ruan, C. Zhou, E. Jin, A. Kucharavy, Y. Zhang, Z. Wen, L. Florens, R. Li, *Nature* **2017**, *543*, 443–446.
[21] K. Tsukakoshi, K. Abe, K. Sode, K. Ikebukuro, *Anal. Chem.* **2012**, *84*, 5542–5547.
[22] C. Tuerk, L. Gold, *Science* **1990**, *249*, 505–510.
[23] A. D. Ellington, J. W. Szostak, *Nature* **1990**, *346*, 818–822.
[24] M. H. Horrocks, M. Palayret, D. Klenerman, S. F. Lee, *Histochem. Cell Biol.* **2014**, *141*, 577–585.
[25] R. Jungmann, C. Steinhauer, M. Scheible, A. Kuzyk, P. Tinnefeld, F. C. Simmel, *Nano Lett.* **2010**, *10*, 4756–4761.
[26] R. Jungmann, M. S. Avendaño, J. B. Woehrstein, M. Dai, W. M. Shih, P. Yin, *Nat. Methods* **2014**, *11*, 313–318.
[27] F. Schueder, J. Lara-Gutiérrez, B. J. Beliveau, S. K. Saka, H. M. Sasaki, J. B. Woehrstein, M. T. Strauss, H. Grabmayr, P. Yin, R. Jungmann, *Nat. Commun.* **2017**, *8*, 2090.
[28] S. J. Sahl, L. E. Weiss, W. C. Duim, J. Frydman, W. E. Moerner, *Sci. Rep.* **2012**, *2*, srep00895.
[29] T. Schlichthaerle, A. Eklund, F. Schueder, M. Strauss, C. Tiede, A. Curd, J. Ries, M. Peckham, D. Tomlinson, R. Jungmann, *Angew. Chem. Int. Ed.* **n.d.**, *0*, DOI 10.1002/anie.201804020.
[30] A. Sharonov, R. M. Hochstrasser, *Proc. Natl. Acad. Sci.* **2006**, *103*, 18911–18916.
[31] C. Soto, *Nat. Rev. Neurosci.* **2003**, *4*, 49–60.
[32] C. Haass, D. J. Selkoe, *Nat. Rev. Mol. Cell Biol.* **2007**, *8*, 101–112.
[33] I. Benilova, E. Karran, B. De Strooper, *Nat. Neurosci.* **2012**, *15*, 349–357.
[34] M. Andreasen, N. Lorenzen, D. Otzen, *Biochim. Biophys. Acta BBA - Biomembr.* **2015**, *1848*, 1897–1907.
[35] M. Serra-Batiste, M. Ninot-Pedrosa, M. Bayoumi, M. Gairí, G. Maglia, N. Carulla, *Proc. Natl. Acad. Sci.* **2016**, *113*, 10866–10871.
[36] J. J. Zarranz, J. Alegre, J. C. Gómez-Esteban, E. Lezcano, R. Ros, I. Ampuero, L. Vidal, J. Hoenicka, O. Rodriguez, B. Atarés, et al., *Ann. Neurol.* **2004**, *55*, 164–173.
[37] S. Lesage, M. Anheim, F. Letournel, L. Bousset, A. Honoré, N. Rozas, L. Pieri, K. Madiona, A. Dürr, R. Melki, et al., *Ann. Neurol.* **2013**, *73*, 459–471.
[38] P. Flagmeier, G. Meisl, M. Vendruscolo, T. P. J. Knowles, C. M. Dobson, A. K. Buell, C. Galvagnion, *Proc. Natl. Acad. Sci.* **2016**, *113*, 10328–10333.
[39] M. H. Polymeropoulos, C. Lavedan, E. Leroy, S. E. Ide, A. Dehejia, A. Dutra, B. Pike, H. Root, J. Rubenstein, R. Boyer, et al., *Science* **1997**, *276*, 2045–2047.
[40] R. Krüger, W. Kuhn, T. Müller, D. Woitalla, M. Graeber, S. Kösel, H. Przuntek, J. T. Epplen, L. Schöls, O. Riess, *Nat. Genet.* **1998**, *18*, 106–108.
[41] M.-C. Chartier-Harlin, J. Kachergus, C. Roumier, V. Mouroux, X. Douay, S. Lincoln, C. Levecque, L. Larvor, J. Andrieux, M. Hulihan, et al., *Lancet Lond. Engl.* **2004**, *364*, 1167–1169.
[42] A. B. Singleton, M. Farrer, J. Johnson, A. Singleton, S. Hague, J. Kachergus, M. Hulihan, T. Peuralinna, A. Dutra, R. Nussbaum, et al., *Science* **2003**, *302*, 841–841.
[43] G. S. Kaminski Schierle, S. van de Linde, M. Erdelyi, E. K. Esbjörner, T. Klein, E. Rees, C. W. Bertoncini, C. M. Dobson, M. Sauer, C. F. Kaminski, *J. Am. Chem. Soc.* **2011**, *133*, 12902–12905.
[44] E. K. Esbjörner, F. Chan, E. Rees, M. Erdelyi, L. M. Luheshi, C. W. Bertoncini, C. F. Kaminski, C. M. Dobson, G. S. Kaminski Schierle, *Chem. Biol.* **2014**, *21*, 732–742.
[45] M. J. Roberti, J. Fölling, M. S. Celej, M. Bossi, T. M. Jovin, E. A. Jares-Erijman, *Biophys. J.* **2012**, *102*, 1598–1607.
[46] M. M. Apetri, R. Harkes, V. Subramaniam, G. W. Canters, T. Schmidt, T. J. Aartsma, *PLoS ONE* **2016**, *11*, DOI 10.1371/journal.pone.0153020.
[47] D. Pinotsi, C. H. Michel, A. K. Buell, R. F. Laine, P. Mahou, C. M. Dobson, C. F. Kaminski, G. S. Kaminski Schierle, *Proc. Natl. Acad. Sci. U. S. A.* **2016**, *113*, 3815–3819.
[48] J. Brelstaff, M. G. Spillantini, A. M. Tolkovsky, *Neural Regen. Res.* **2015**, *10*, 1746–1747.
[49] J. Brelstaff, B. Ossola, J. J. Neher, T. Klingstedt, K. P. R. Nilsson, M. Goedert, M. G. Spillantini, A. M. Tolkovsky, *Front. Neurosci.* **2015**, *9*, DOI 10.3389/fnins.2015.00184.
[50] L. B. Lassen, E. Gregersen, A. K. Isager, C. Betzer, R. H. Kofoed, P. H. Jensen, *PLOS ONE* **2018**, *13*, e0196056.